IEEE Control Systems Letters paper presented at
2023 American Control Conference (ACC)
San Diego, CA, USA. May 31 - June 2, 2023

Implementation and Initial Testing of a Model Predictive Controller for Safety Factor Profile and Energy Regulation in the EAST Tokamak*

Zibo Wang[1], Hexiang Wang[2], Eugenio Schuster[1], Zhengping Luo[3], Yao Huang[3], Qiping Yuan[3], Bingjia Xiao[3], David Humphreys[4], and Sai Tej Paruchuri[1]

***Abstract*— The tokamak, a potential candidate for realizing nuclear fusion energy on Earth, uses strong magnetic fields to confine a hot ionized gas (plasma) in a toroidal vacuum chamber. The ability of tokamaks to run in high-performance modes of operation demands advanced control capabilities to regulate the spatial distribution (profile) of several plasma properties such as the safety factor q. A model predictive control (MPC) approach has been followed to further advance such control capabilities for the EAST tokamak. The proposed controllers have the capability of simultaneously regulating the q-profile and the plasma stored energy W by controlling the plasma current I_p, the individual powers of four neutral beam injectors (NBI_{1L}, NBI_{1R}, NBI_{2L}, NBI_{2R}), and the powers of two lower hybrid wave sources with different frequencies (2.45 GHz, 4.60 GHz). An active-set algorithm has been employed to solve the Quadratic Programming (QP) problem arising from the MPC formulation. Initial experimental tests of the MPC show that the real-time optimization is successfully carried out within the time constraints imposed by the dynamics of the plasma.**

I. INTRODUCTION

As an energy source, nuclear fusion offers many advantages such as a high energy density, a nearly inexhaustible source of fuel, no air pollution or greenhouse gases, a relatively short lived radioactive waste, and no risk of a nuclear accident (meltdown). Nuclear fusion is achieved by fusing together two light nuclei to form one heavier nucleus. This process releases an enormous amount of energy. In order to overcome the Coulomb repulsion force and make the two nuclei fuse, a tremendous amount of kinetic energy must be given to the nuclei by raising the temperature of the gas fuel to around 100 million degrees. In such a high-temperature environment, the gas is ionized and turned into a plasma, also referred to as the fourth state of matter. Since the plasma is too hot to be in contact with the inner wall of any type of container, a tokamak device confines it in a toroidal vacuum chamber by generating strong magnetic fields that balance the expansion pressure of the plasma.

Tokamak operation at a high fusion gain for sufficiently long periods of time will most likely require to be operated under what are called advanced tokamak (AT) scenarios.

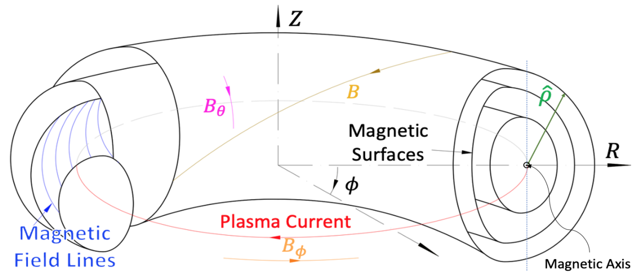

Fig. 1. Magnetic configuration. Poloidal ($\bar{B}_\theta$) and toroidal ($\bar{B}_\Phi$) magnetic fields are combined to produce a helical magnetic field $\bar{B}$, which confines the toroidal plasma. On a poloidal plane of the torus, each point is identified by a value of the poloidal magnetic flux $\Psi(R,Z)$. Around the magnetic axis, points with identical $\Psi(R,Z)$ values define nested magnetic flux surfaces. Any quantity indexing these flux surfaces from the magnetic axis to the plasma boundary could be adopted as the spatial coordinate $\hat{\rho}$.

These AT scenarios are characterized by improved confinement, magneto-hydro-dynamic (MHD) stability, and possible steady-state operation. It has been demonstrated that the realization of AT scenarios is linked to the capability of shaping the spatial distribution, or simply the "profile," of several plasma properties such as the safety factor q, which is a measurement of the pitch of the helical magnetic field lines confining the hot plasma. Auxiliary heating, both non-inductive and inductive current drives, and particle injection can be used as actuators for profile control.

Initial work on q-profile control followed a non-model-based approach but it was soon realized that the high-dimensionality and nonlinearity of the problem demanded a model-based approach. Since then, the problem has attracted a great deal of attention and several solutions have been proposed, including approaches like robust control [1], [2], [3], optimal control [4], [5], Lyapunov-based control [6], [7], and model predictive control (MPC) [8], [9], [10]. In spite of the significant progress, several aspects of the MPC problem remain open due in part to the gap between synthesis and implementation, arising from the high computational demands of the MPC scheme in relation to the relatively short length of present tokamak discharges (order of seconds). Building on the results in [10], an MPC algorithm is proposed in this work to regulate the q-profile and the plasma stored energy W at the Experimental Advanced Superconducting Tokamak (EAST) tokamak. The synthesis of the controller rests on a first-principles-driven (FPD), control-oriented model of the safety-factor dynamics [11], which is governed by a partial differential equation (PDE) known as the magnetic diffusion equation (MDE). To capture the energy dynamics, the model is augmented with a zero-dimensional power balance in

*This work was supported in part by the U.S. Department of Energy under contract DE-SC0010537.

[1]Z. Wang (zibo.wang@lehigh.edu), H. Wang, E. Schuster, and S. T. Paruchuri are with the Department of Mechanical Engineering and Mechanics, Lehigh University, Bethlehem, PA 18015, USA.

[2]H. Wang is with the Shanghai Institute of Applied Physics, Chinese Academy of Sciences, Shanghai 201800, PRC.

[3]Z. Luo, Y. Huang, Q. Yuan, and B. Xiao are with the Institute of Plasma Physics, Chinese Academy of Sciences, Hefei 230031, PRC.

[4]D. Humphreys is with General Atomics, San Diego, CA 92121, USA.

the form of an ordinary differential equation (ODE). The dimensionality of the response model is reduced by using a finite-difference approximation on a uniform grid. Further linearization of the nonlinear dynamics leads to a set of ODEs capturing the linearized dynamics of the q-profile and the plasma energy W, which are used as constraints for the MPC-related optimization problem. One of the main contributions of this work is the implementation of a real-time optimization solver within the newly created Profile Control category in the EAST Plasma Control System (PCS) to solve the MPC problem. The total plasma current, together with the individual powers of different current drives (neutral beam injection (NBI), lower hybrid wave (LHW)), are directly commanded by the controller running within the Profile Control category. The q profile and W are computed in real-time from magnetic measures in EAST via the equilibrium reconstruction algorithm p-EFIT [12]. The performance of the real-time optimizer has been tested both in PCS-in-the-loop nonlinear simulations and experiments. However, the results for the PCS-in-the-loop nonlinear simulations, which show the controller is correctly implemented and its ability to precisely and reliably achieve a desired trajectory, are omitted in this paper due to the page limitation. Initial experimental tests, which focused on assessing the feasibility of solving the MPC optimization problem in real time and not on demonstrating tracking performance, show that the MPC algorithm is ready for physics-oriented experiments.

This paper is organized as follows. In Section II, the response models for q and W are introduced. Details on the model reduction and linearization process are provided in Section III. In Section IV, the control-oriented model is used as a dynamic constraint for the optimization problem arising from the MPC formulation. A quadratic programming (QP) solver for the solution of the optimization problem in real time is also presented in this section. Initial experimental results from the EAST tokamak illustrating the feasibility of the real-time optimization algorithm to regulate the safety factor and plasma stored energy is presented in Section V. Conclusions and future works are discussed in Section VI.

II. POLOIDAL MAGNETIC FLUX AND ENERGY EVOLUTION MODELS

The helical magnetic field $\bar{B}$ confining the plasma is the sum of the toroidal, $\bar{B}_\phi$, and poloidal, $\bar{B}_\theta$, components (i.e., $\bar{B} = \bar{B}_\phi + \bar{B}_\theta$). The geometry of the magnetic configuration in a tokamak is illustrated Fig. 1 by using a cylindrical coordinate system defined by (R, Z, ϕ). The poloidal magnetic flux Ψ at a point P within the tokamak is calculated as $\Psi \triangleq \int_S \bar{B}_\theta \cdot d\bar{S}$. The surface S is perpendicular to the Z axis and its boundary is defined by a circular ring crossing the point P. Points of identical Ψ values define nested magnetic-flux surfaces as illustrated in Fig. 1. Any quantity indexing these flux surfaces from the magnetic axis to the plasma boundary can be adopted as spatial coordinate ρ. The spatial coordinate in this work is chosen as the mean effective minor radius, $\rho \triangleq \sqrt{\Phi/(B_{\phi,0}\pi)}$, where $B_{\phi,0}$ is the vacuum toroidal magnetic field at the major radius, R_0. The toroidal magnetic flux, Φ, is defined as $\Phi \triangleq \int_{S_\phi} \bar{B}_\phi \cdot d\bar{S}_\phi$, where S_ϕ is the surface perpendicular to the ϕ axis whose boundary is the magnetic-flux surface defined by P. The normalized mean effective minor radius is defined as $\hat{\rho} \triangleq \rho/\rho_b$, where ρ_b is the mean effective minor radius of the last-closed plasma boundary. The spatial 3D problem is reduced to a 1D problem by using this spatial coordinate in combination with the assumption of toroidal symmetry.

A. Poloidal Magnetic Flux Dynamics

The magnetic diffusion equation (MDE) governs the evolution of the stream function defined as $\psi \triangleq \Psi/2\pi$, i.e.

$$\frac{\partial \psi}{\partial t} = \frac{\eta(T_e)}{\mu_0 \rho_b^2 \hat{F}^2} \frac{1}{\hat{\rho}} \frac{\partial}{\partial \hat{\rho}} \left(\hat{\rho} D_\psi \frac{\partial \psi}{\partial \hat{\rho}} \right) + R_0 \hat{H} \eta(T_e) \frac{\langle \bar{j}_{NI} \cdot \bar{B} \rangle}{B_{\phi,0}}, \quad (1)$$

with two given boundary conditions, $\frac{\partial \psi}{\partial \hat{\rho}}|_{\hat{\rho}=0} = 0$ and $\frac{\partial \psi}{\partial \hat{\rho}}|_{\hat{\rho}=1} = k_{I_p} I_p$, where I_p is the plasma current, μ_0 is the permeability in vacuum, and $\hat{F}$, $\hat{G}$ and $\hat{H}$ are geometric factors. The angle bracket $\langle \rangle$ is used to denote the flux-surface average of a quantity. Control-oriented models are used for the electron temperature and density (T_e and n_e), ion temperature and density (T_i and n_i), plasma resistivity η, and non-inductive current-drive $\frac{\langle \bar{j}_{NI} \cdot \bar{B} \rangle}{B_{\phi,0}}$, which are needed for closure of the MDE [11]. The terms D_ψ and k_{I_p} are defined as $D_\psi(\hat{\rho}) \triangleq \hat{F}(\hat{\rho}) \hat{H}(\hat{\rho}) \hat{G}(\hat{\rho}), k_{I_p} \triangleq -\frac{\mu_0}{2\pi} \frac{R_0}{\hat{G}(1)\hat{H}(1)}$. The safety factor profile is written as $q(\hat{\rho}, t) = -B_{\phi,0} \rho_b^2 \hat{\rho} (\frac{\partial \psi}{\partial \hat{\rho}})^{-1}$.

Details on how control-oriented models for the ion densities and temperatures, the electron densities and temperatures, the plasma resistivity $\eta(T_e)$, the non-inductive current drive (j_{NI}), and the bootstrap current are developed for the EAST tokamak can be found in [2], [5]. These control-oriented models allow the MDE (1) to be rewritten as

$$\frac{\partial \psi}{\partial t} = \left(C_{f_1} \frac{\partial \psi}{\partial \hat{\rho}} + C_{f_2} \frac{\partial^2 \psi}{\partial \hat{\rho}^2} \right) u_{diff} + \sum_i C_{j_i} u_{j_i} + C_{j_{bs}} \left(\frac{\partial \psi}{\partial \hat{\rho}} \right)^{-1} u_{j_{bs}},$$

which can in turn be further rewritten in terms of the poloidal magnetic flux gradient, which is defined as $\theta \triangleq \partial \psi / \partial \hat{\rho}$), i.e.

$$\frac{\partial \theta}{\partial t} = \left[\frac{dC_{f_1}}{d\hat{\rho}} \theta + \left(C_{f_1} + \frac{dC_{f_2}}{d\hat{\rho}} \right) \frac{\partial \theta}{\partial \hat{\rho}} + C_{f_2} \frac{\partial^2 \theta}{\partial \hat{\rho}^2} \right] u_{diff} + \sum_i \frac{dC_{j_i}}{d\hat{\rho}} u_{j_i} + \frac{dC_{j_{bs}}}{d\hat{\rho}} \frac{1}{\theta} u_{j_{bs}} - C_{j_{bs}} \frac{1}{\theta^2} \frac{\partial \theta}{\partial \hat{\rho}} u_{j_{bs}} \triangleq f_\theta, \quad (2)$$

where $i \in [nbi_1, \cdots, nbi_{n_{nbi}}, lhw_1, \cdots, lhw_{n_{lhw}}]$, $C_{f_1}, C_{f_2}, C_{j_i}$, and $C_{j_{bs}}$ are function of $\hat{\rho}$, n_{nbi} and n_{lhw} are the number of NBI and LHW injection sources, respectively. The boundary conditions are rewritten as $\theta|_{\hat{\rho}=0} = 0, \theta|_{\hat{\rho}=1} = k_{I_p} I_p$. The virtual control inputs u_{diff}, u_{j_i} and $u_{j_{bs}}$ are defined as functions of I_p, total injected power P_{tot}, and line-averaged density $\bar{n}_e$ [5]:

$$u_{diff}(t) \triangleq \sqrt{I_p(t)^{-3\gamma} P_{tot}(t)^{-3\varepsilon} \bar{n}_e(t)^{-3\zeta}}, \quad (3)$$

$$u_{j_i}(t) \triangleq \bar{n}_e(t)^{(\zeta(\delta-1.5)-1)} \left(I_p(t)^\gamma P_{tot}(t)^\varepsilon \right)^{(\delta-1.5)} P_i(t), \quad (4)$$

$$u_{j_{bs}}(t) \triangleq I_p(t)^{-0.5\gamma} P_{tot}(t)^{-0.5\varepsilon} \bar{n}_e(t)^{1-0.5\zeta}. \quad (5)$$

B. Plasma Stored Energy Dynamics

A nonlinear first-order equation is used to approximately model the dynamics of the volume-averaged plasma stored energy density, i.e. $\frac{dW}{dt} = -\frac{W}{\tau_E(t)} + P_{tot}(t) \triangleq f_W$, where $\tau_E \propto I_p(t)^{0.96} P_{tot}(t)^{-0.73} \bar{n}_e(t)^{0.4}$ denotes the energy confinement time, which in this work is based on the $IPB98(y,2)$ [13].

III. CONTROL-ORIENTED MODEL FOR MPC

A. Model Reduction via Finite Difference

A finite-dimensional model can be obtained by discretizing the infinite-dimensional system described by the PDE (2) on a uniform spatial grid. The points of this uniform grid are defined as $\hat{\rho}_i \triangleq (i-1)/(k-1)$, where $i \in \{1,\cdots,k\}$ and k is the number of grid points. The symbol θ_i is used to denote θ at $\hat{\rho}_i$. Over the interior nodes $(\hat{\rho}_2,\cdots,\hat{\rho}_{k-1})$, the spatial derivatives of θ are approximated by second-order Taylor series expansions. By defining $Z \triangleq [\theta_1, \theta_2, \cdots, \theta_{n-1}, \theta_n, W]^T \in \mathbb{R}^{(k+1)\times 1}$ and $F \triangleq [f_\theta, f_W]$, the discretized dynamic model is written as $\dot{Z} = F(Z,u)$, where $u \triangleq [u_{diff}, u_{j_{bs}}, u_{j_{nbi_1}}, \cdots, u_{j_{nbin_{nbi}}}, u_{j_{lhw_1}}, \cdots, u_{j_{lhwn_{lh}}}, I_p]^T$.

B. Derivation of Offset-free Error Model

The dynamic model $\dot{Z} = F(Z,u)$ is linearized around a given reference trajectory (Z_{ref}, u_{ref}) by using a first-order Taylor series expansion, i.e.

$$\dot{Z} \approx F(Z_{ref}, u_{ref}) + \left.\frac{\partial F}{\partial Z}\right|_{(Z_{ref},u_{ref})} (Z - Z_{ref}) + \left.\frac{\partial F}{\partial u}\right|_{(Z_{ref},u_{ref})} (u - u_{ref}). \quad (6)$$

The reference trajectory is assumed stationary (for instance, a stationary profile obtained during the flattop current phase under constant inputs. This simplifying approximation leads to a linear time-invariant (LTI) model.

By recalling that $\dot{Z}_{ref} = F(Z_{ref}, u_{ref})$ and defining $\Delta Z \triangleq Z - Z_{ref}$, $\Delta u \triangleq u - u_{ref}$, (6) is written as

$$\Delta \dot{Z} = A \Delta Z + B \Delta u, \quad (7)$$

where $A \in \mathbb{R}^{(k+1)\times(k+1)}$ and $B \in \mathbb{R}^{(k+1)\times 1}$ are the Jacobian matrices of F with respect to Z and u evaluated at (Z_{ref}, u_{ref}), respectively. A discrete-time systems

$$\Delta Z^{j+1} = A_1 \Delta Z^j + B_1 \Delta u^j \quad (8)$$

is obtained by discretizing the system (7) on a temporal grid $t_j = j\Delta t$, where $j \in [0,1,\cdots]$, Δt is the time interval of the discrete-time systems, $A_1 \triangleq \Delta t A + I$, and $B_1 \triangleq \Delta t B$. The values of ΔZ and Δu evaluated at $t = t_j$ are denoted as ΔZ^j and Δu^j. In order to incorporate integral action to achieve offset-free tracking, (8) is rewritten in velocity form:

$$d\Delta Z^{j+1} = A_1 d\Delta Z^j + B_1 d\Delta u^j, \quad (9)$$

where $d\Delta Z^{j+1} \triangleq \Delta Z^{j+1} - \Delta Z^j$ and $d\Delta u^{j+1} \triangleq \Delta u^{j+1} - \Delta u^j$. By denoting the desired states at $t = t_j$ as Z^j_{tar}, ΔZ^j_{tar} is defined as $\Delta Z^j_{tar} \triangleq Z^j_{tar} - Z^j_{ref}$. Therefore, if the prediction is carried out from $t = t_j$, the tracking error at $t = t_{j+n}$ is written in discretized form as (note that $\Delta Z^{j+n} = \Delta Z^j + \sum_{i=j+1}^{j+n} d\Delta Z^i$)

$$\Delta Z^{j+n} - \Delta Z^{j+n}_{tar} = \Delta Z^j + \sum_{i=j+1}^{j+n} d\Delta Z^i - \Delta Z^{j+n}_{tar}. \quad (10)$$

IV. MODEL PREDICTIVE CONTROL FOR EAST

A. Control Input Constraints

The vector of physical inputs (i.e., I_p, power of four neutral beam injectors and two lower hybrid waves) is defined as $u_p \triangleq [I_p, P_{NBI_{1L}}, P_{NBI_{1R}}, P_{NBI_{2L}}, P_{NBI_{2R}}, P_{LH_1}, P_{LH_2}]^T$. And the constraints on both u_p and the I_p rate of change at time $t = t_j$ can be written as

$$u_p^{min} \preceq u_p^j \preceq u_p^{max}, \quad dI_p^{min} \leq \left.\frac{dI_p}{dt}\right|_j \leq dI_p^{max}, \quad (11)$$

where $u_p^{min} \in \mathbb{R}^{7\times 1}$ and $u_p^{max} \in \mathbb{R}^{7\times 1}$ are the lower and upper bounds of u_p^j, dI_p^{min} and dI_p^{max} are the minimum and maximum rates of change of I_p. Based on (3)-(5), the connection between the virtual control inputs u^j and the physical inputs u_p^j is given by the invertible nonlinear transformation function g_{nt} and written as $u^j \triangleq g_{nt}(u_p^j)$. By computing a first-order Taylor series expansion of it, $\Delta u^j \triangleq u^j - u_{ref}$ and $d\Delta u^j \triangleq \Delta u^j - \Delta u^{j-1}$ should satisfy

$$\Delta u^j = \left.\frac{\partial g_{nt}}{\partial u_p}\right|_{u_{p,ref}} \Delta u_p^j, \quad d\Delta u^j = \left.\frac{\partial g_{nt}}{\partial u_p}\right|_{u_{p,ref}} d\Delta u_p^j, \quad (12)$$

with $g_{nt}(u_{p,ref}) \triangleq u_{ref}$, $\Delta u_p^j \triangleq u_p^j - u_{p,ref}$, $d\Delta u_p^j \triangleq \Delta u_p^j - \Delta u_p^{j-1}$.

B. Formulation of MPC Problem

A deviation vector that concatenates incremental deviation states and control inputs at $t = t_j$ is defined as $X_j \triangleq [(d\Delta u_p{}^j)^T, (d\Delta Z^{j+1})^T]^T \in \mathbb{R}^{(k+8)\times 1}$. Since the goal is to minimize the tracking error and the feedback control effort over a receding horizon, the to-be-minimized cost function is

$$J = \sum_{n=j}^{j+N_p-1} \frac{(\Delta Z^{n+1} - \Delta Z^{n+1}_{tar})^T Q_n (\Delta Z^{n+1} - \Delta Z^{n+1}_{tar})}{2} + (\Delta u_p^n)^T R_n \Delta u_p^n,$$

where Q_n and R_n are positive-definite weighting matrices.

By grouping deviation variables for the optimization problem from the present time step $t = t_j$ to the final predicted time step $t = t_{j+N_p}$, i.e. $\bar{X} \triangleq [X_j, X_{j+1}, \cdots, X_{j+N_p-1}]^T \in \mathbb{R}^{[(k+8)\cdot N_p]\times 1}$. And using linear algebra, the velocity form of the system model (9), the constraints on the physical actuators, and the cost function can be written as a linearly constrained quadratic optimization problem. Thus, solving this problem implies finding a feasible $\bar{X}^*$ that satisfies

$$\min_{\bar{X}} \quad \frac{1}{2} \bar{X}^T P \bar{X} + f \cdot \bar{X} \quad (13)$$

$$\text{s.t.} \quad b_{eq} = A_{eq} \bar{X}, \quad b_{in} \succeq A_{in} \bar{X}, \quad (14)$$

where $P \in \mathbb{R}^{[(k+8)\cdot N_p]\times[(k+8)\cdot N_p]}$ is a positive-definite diagonal matrix and $f \in \mathbb{R}^{1\times[(k+8)\cdot N_p]}$ is a row vector. The equality constraint in (14) is formulated by combining (9) and (12) over the prediction horizon, where $A_{eq} \in \mathbb{R}^{[(k+8)\cdot N_p]\times[(k+8)\cdot N_p]}$ and $b_{eq} \in \mathbb{R}^{[(k+8)\cdot N_p]\times 1}$. The inequality constraint in (14) is a variation of (11) over the prediction horizon, where $A_{in} \in \mathbb{R}^{14N_p\times[(k+8)\cdot N_p]}$ and $b_{in} \in \mathbb{R}^{14N_p\times 1}$.

C. Quadratic Programming for Solving MPC Problem

The efficiency to solve the quadratic programming (QP) problem (13)-(14) determines the feasibility of implementing the MPC algorithm in real-time applications. In this work, the method used to solve the QP problem is the active-set method, which is based on the Lagrange multiplier method. This choice is justified by the low number of variables needed to formulate the optimization problem. Thus, the computational power required for each iteration is relatively small. This is important for profile control in EAST since the control law needs to be updated every 10 *ms*.

The value of the elements in the active-set $\mathscr{A} \in \mathbb{R}^{1\times 14N_p}$ are either 0 or 1. If the i^{th} element in $\mathscr{A}$ is 1, it indicates that the solution resides at the boundary of the inequality (i.e., $b_{in}^i = A_{in}^i \bar{X}^*$, where the i^{th} row of the matrix A_{in} is written as A_{in}^i, and the i^{th} element of b_{in} is denoted by b_{in}^i). The set $\mathscr{I}$ contains the indices of all the non-zero terms in $\mathscr{A}$.

By using the Lagrangian form, the QP problem defined in (13) to (14) is written as

$$\min_{\bar{X}} \mathscr{L} \triangleq \frac{\bar{X}^T P \bar{X}}{2} + f\cdot\bar{X} + \sum_i^m \lambda_i \left(A_{eq}^i \bar{X} - b_{eq}^i\right) + \sum_{i\in\mathscr{I}}^r \nu_i \left(A_{in}^i \bar{X} - b_{in}^i\right),$$

where λ_i is the Lagrange multiplier associated with $\left(A_{eq}^i \bar{X} - b_{eq}^i\right) = 0$, ν_i is the Lagrange multiplier associated with $\left(A_{in}^i \bar{X} - b_{in}^i\right) \leq 0$, and m is the number of row in A_{eq}. Because the inequality constraint introduced in (11) has lower and upper bounds, the matrix A_{in} can be divided into two parts, $A_{in,lb} \in \mathbb{R}^{n_{lb}\times[(k+8)\cdot N_p]}$ and $A_{in,ub} \in \mathbb{R}^{n_{ub}\times[(k+8)\cdot N_p]}$. The matrix $A_{in,lb}$ is related to the lower bounds, while the matrix $A_{in,ub}$ is related to the upper bounds. The numbers of rows in $A_{in,lb}$ and $A_{in,ub}$ are noted as n_{lb} and n_{ub}, where $n_{lb} + n_{ub} = r$. Similarly, the vector b_{in} is also split into $b_{in,lb}$ and $b_{in,ub}$, while the vector ν is split into ν_{lb} and ν_{ub}. The sets $\mathscr{V}_{lb}$ and $\mathscr{V}_{ub}$ contain the indices of the active lower-bound and upper-bound constraints, respectively.

The Karush-Kuhn-Tucker (KKT) conditions are used to ensure that this nonlinear optimization problem has a feasible solution. The first-order KKT condition can be written as

$$P\bar{X}^* + f^T + \sum_i^m \lambda_i \left(A_{eq}^i\right)^T + \sum_{i\in\mathscr{I}}^r \nu_i \left(A_{in}^i\right)^T = 0, \quad (15)$$

$$b_{eq} = A_{eq}\bar{X}^*, \quad b_{in}^i = A_{in}^i \bar{X}^*, \quad \forall i \in \mathscr{I}, \quad (16)$$

$$b_{in} \succeq A_{in}\bar{X}^*, \quad \nu_i \geq 0, \quad \forall i \in \mathscr{I}. \quad (17)$$

The second-order KKT condition is automatically satisfied since the weighting matrix P is positive-definite. The solution to (15)-(16) can be computed from the linear system

$$\begin{bmatrix} P & A_{eq}^T & A_{in,act}^T \\ A_{eq} & 0 & 0 \\ A_{in,act} & 0 & 0 \end{bmatrix} \begin{bmatrix} \bar{X}^* \\ \lambda \\ \nu_{act} \end{bmatrix} = \begin{bmatrix} -f^T \\ b_{eq} \\ b_{in,act} \end{bmatrix}, \quad (18)$$

where $A_{in,act}$ is the matrix composed by the rows of A_{in} indexed by the set $\mathscr{I}$. Similarly, $b_{in,act}$ and ν_{act} are the vectors composed by the elements of b_{in} and ν indexed by the set $\mathscr{I}$. By defining a new matrix $\tilde{A} \triangleq [A_{eq}, A_{in,act}]^T$ and new vectors $\tilde{b} \triangleq [b_{eq}, b_{in,act}]^T$ and $\omega \triangleq [\lambda, \nu_{act}]^T$, the solution of (18) for ω and $\bar{X}^*$ can be written as

$$\omega = \left(\tilde{A}P^{-1}\tilde{A}^T\right)^{-1}\left(-\tilde{b} - \tilde{A}P^{-1}f^T\right), \bar{X}^* = -P^{-1}\left(f^T + \tilde{A}^T\omega\right). \quad (19)$$

However, depending on the selection of the current active-set, $[\omega, \bar{X}^*]^T$ may not necessarily satisfy (17). The parts that violate (17) need to be considered in (16), and the parts causing invalid Lagrange multipliers should be removed from (16). Therefore, solving the optimization problem implies solving (15)-(16) iteratively until no violation for (17) is found. The summary of the active-set algorithm can be found in Algorithm 1. It starts with an initial guess for the active-set $\mathscr{A}_0$. After solving ω and $\bar{X}^*$, the conditions (17) are checked. Zero vectors i_{lb}^L, i_{lb}^P, and i_{lb}^{min} are initialized for every iteration, where $i_{lb}^L = i_{lb}^P = i_{lb}^{min} = \overrightarrow{0} \in \mathbb{R}^{1\times n_{lb}}$. The algorithm sets the i^{th} element in i_{lb}^L to 1 if the positive condition for the Lagrange multipliers is violated, flagging the variables that should not have been bounded and need to be removed. Then the algorithm sets the i^{th} element in i_{lb}^P to 1 if the $A_{in,lb}^i \bar{X} \leq b_{in,lb}$ conditions is violated. The vector i_{lb}^{min} is computed as $(i_{lb}^P - i_{lb}^L)$, but only the first non-zero term is kept. A positive value in i_{lb}^{min} means the variable may need to be added to a candidate active-set, while a negative value means the variable may need to be removed. The same approach is applied to the upper bounds. Zero vectors i_{ub}^L, i_{ub}^P, and i_{ub}^{min} that have same size as $\nu_{act,ub}$ are initialized. The algorithm sets the i^{th} element in i_{ub}^L to 1 if the condition $\nu_{act,ub}^i \geq 0$ is violated and sets the i^{th} element in i_{ub}^P to 1 if the $A_{in,ub}^i \bar{X} \leq b_{in,ub}$ condition is violated. Then, i_{ub}^{min} is computed as $(i_{ub}^P - i_{ub}^L)$, but only the first non-zero term is kept. By comparing the indices of non-zero terms in i_{lb}^{min} and i_{ub}^{min}, the vector with the smaller index is kept and the non-zero index indicates where the current active set $\mathscr{A}_0$ needs to be adjusted. The vector with the larger index is reset to zero. Through this method, only one part of the constraints, either the lower bounds or the upper bounds, is taken into account in a single iteration. A working vector is then defined as $\mathscr{W} \triangleq [i_{lb}^{min}, i_{ub}^{min}]$. Then, a newly amended active-set is obtained by adding $\mathscr{W}$ to the current one. This procedure is repeated until no violation is found for (17) or the iteration number reaches the maximum number.

In practice, the number of iterations required by the active-set algorithm is usually less than 10, which takes about 10 μs in the PCS. It is worth noting, however, that the Algorithm 1 may terminate before getting the optimal solution (i.e., the maximum iteration number is reached), and the solution may not be feasible. If this kind of failure happened, the physical inputs would not be bounded. However, in this case the power requests would be constrained by the minimum or maximum values imposed by the saturation block in series with the controller, not causing any operational damage.

V. EXPERIMENTAL RESULT OF MPC

This section presents very preliminary experimental results from a recent EAST campaign. Electron Cyclotron Range of Frequency (ECRF) heating was used during the experiments to keep the operation in H-mode (high-confinement mode).

Algorithm 1: Active-Set Algorithm for QP Problem

$iter \longleftarrow 0$, start with a candidate active-set $\mathscr{A}_0$;
repeat
  Initialize $\mathscr{W}$, i_{lb}^L, i_{lb}^P, i_{lb}^{min}, i_{ub}^L, i_{ub}^P, and i_{ub}^{min} to $\overrightarrow{0}$
  Solve for ω and $\bar{X}^*$ using (19)
  if $v_{lb}^i < 0 \; \exists i \in \mathscr{I}_{lb}$ **then**
    Set the i^{th} element in i_{lb}^L to 1
  if $A_{in,lb}^i \bar{X} > b_{in,lb} \; \exists i \in \mathscr{V}_{lb}$ **then**
    Set the i^{th} element in i_{lb}^P to 1
  if $v_{ub}^i < 0 \; \exists i \in \mathscr{I}_{ub}$ **then**
    Set the i^{th} element in i_{ub}^L to 1
  if $A_{in,ub}^i \bar{X} > b_{in,ub} \; \exists i \in \mathscr{V}_{ub}$ **then**
    Set the i^{th} element in i_{ub}^P to 1
  Compute $\mathscr{W}$ **if** $\mathscr{W} \neq \overrightarrow{0}$ **then**
    $\mathscr{A}_{iter+1} \longleftarrow \mathscr{A}_{iter} + \mathscr{W}$
  else
    return the current $\mathscr{A}_{iter}$
  if $iter <$ *maximum iteration number* **then**
    $iter \longleftarrow iter + 1$
until *(17) are satisfied simultaneously or* $iter \geq$ *maximum iteration number*
$\mathscr{A} \longleftarrow \mathscr{A}_{iter}$
return $\mathscr{A}$ and $\bar{X}^*$

First, a feedforward-only shot (#103719) was executed. Second, feasible q-profile and plasma stored energy W target evolutions were obtained by executing another feedforward-only shot (#103720) with an input set different from that used in shot #103719. The feedforward + feedback shot (#103739) was run with the same feedforward inputs used in shot #103719 but using the targets generated in shot #103720. Feedback control is needed in this case to correct the feedforward inputs and effectively track the target q and W evolutions. The number of grid points for the $\hat{\rho}$ coordinate was adopted as 21 and the prediction horizon was chosen as 2. The controller sent requests only for I_p, P_{LH_1}, and P_{LH_2}. The input ranges were predefined as $I_p \in [0.3, 0.6] MA$, $P_{LH_1} \in [0, 0.8]\ MW$, and $P_{LH_2} \in [1.0, 2.9]\ MW$. As shown in Fig. 2, the MPC algorithm was turned on at 2 seconds. The q-profile regulation results are shown in Fig. 2(a)-(c), while the results for the plasma stored energy are presented in Fig. 2(d). Target trajectories are shown in solid red lines; feedforward trajectories are shown in solid magenta lines; feedforward + feedback trajectories are shown in dashed blue lines. In Fig. 2(a)-(b), the targets (red line) are lower than the actual evolutions (blue line), which requires P_{LH_1} and P_{LH_2} (Fig. 2(f)-(g)) to be lower in order to track the targets. However, the powers requested by the MPC algorithm are saturated at their minimum limits, which prevents the q-profile evolutions in Fig. 2(a)-(b) from reaching the target values. Unfortunately, a non-zero $P_{NBI_{1L}}$ value was accidentally delivered in the background to the NBI_{1L} source, as shown in Fig. 2(f), which was indeed supposed to be turned off during this shot as it was turned off during shots #103719 and #103720. The presence of the NBI_{1L} source made the target q-profile generated in shot #103720 no longer feasible, causing the saturation of LHW sources and preventing the controller from achieving the target. The controller slightly increases I_p (Fig. 2(e)) over the feedforward input in order to reduce $q(\hat{\rho} = 0.9)$ (Fig. 2(c)) and drive it closer to the target. The evolution of W (Fig. 2(d)) shows relatively good tracking in spite of the fact that the controller is trying to reduce P_{LH} in order to better track the q-profile in the core. The MPC optimally solves the tradeoff between increasing W (higher P_{LH}) and reducing q in the core (lower P_{LH}).

Another shot (#114118) was conducted to test the capability of the MPC algorithm to command the NBI system, which operates on an on/off basis. During this experiment, only W was controlled by using $P_{NBI_{2R}}$ as an actuator. The feedforward control input was identical to that used in the feedforward-only shot #114099 and the evolution of the feedforward-only shot #114106 was adopted as the target. A pulse width modulation (PWM) algorithm has been implemented in the EAST PCS to convert the requested NBI power P_{NBI} to on/off commands, as required by the operation of the NBI system, by determining the time t_{PW}^{req} that the beam must be on within a cycle t_c. At the expense of introducing some approximation in the requested beam power, the PWM logic shown in Fig. 3 guarantees that the constraints on both the minimum on-time t_{on}^{min}, which is the time that the NBI needs to be kept on before shutting it off, and the minimum off-time t_{off}^{min}, which is the time that the NBI needs to be kept off before turning it on, are satisfied. Given the P_{NBI} request, the pulse width is computed as $t_{PW} \triangleq (P_{NBI}/P_{NBI}^{max}) t_c$, where t_c is the chosen cycle interval and P_{NBI}^{max} is the power delivered by the NBI system when it is turned on. In this experiment, $P_{NBI} = P_{NBI_{2R}}$, which is the output of the MPC algorithm. In spite of the delays associated with the minimum on-time and off-time constraints ($t_{on}^{min} = t_{off}^{min} = 100ms$) over a cycle time of $t_c = 400ms$, the MPC is capable of tracking the desired W target as shown in Fig. 4(left) by correcting the feedforward input as shown in Fig. 4(right). The tracking could be improved by relaxing the safety-related constraints (lower t_{on}^{min} and t_{off}^{min}) and/or by including the discrete-time nature of the actuator in the MPC design (hybrid MPC).

VI. CONCLUSIONS AND FUTURE WORK

A real-time-optimization feedback-control algorithm for simultaneous regulation of the plasma q-profile and stored energy W has been proposed based on the MPC approach. The main contribution of the work is not on the synthesis of the MPC algorithm itself, but on the reduction of the gap between synthesis and implementation at EAST. This is achieved by proposing a real-time optimizer based on the active-set method and connecting the PCS with a nonlinear model to assess in simulations the readiness for experimental testing (simulation results can be provided upon request). Preliminary experimental tests show the effectiveness of the proposed QP solver to find a solution to the MPC problem within the time constraints of the system. Ongoing and future work includes increasing the number of commanded actuators and further testing the performance of the MPC.

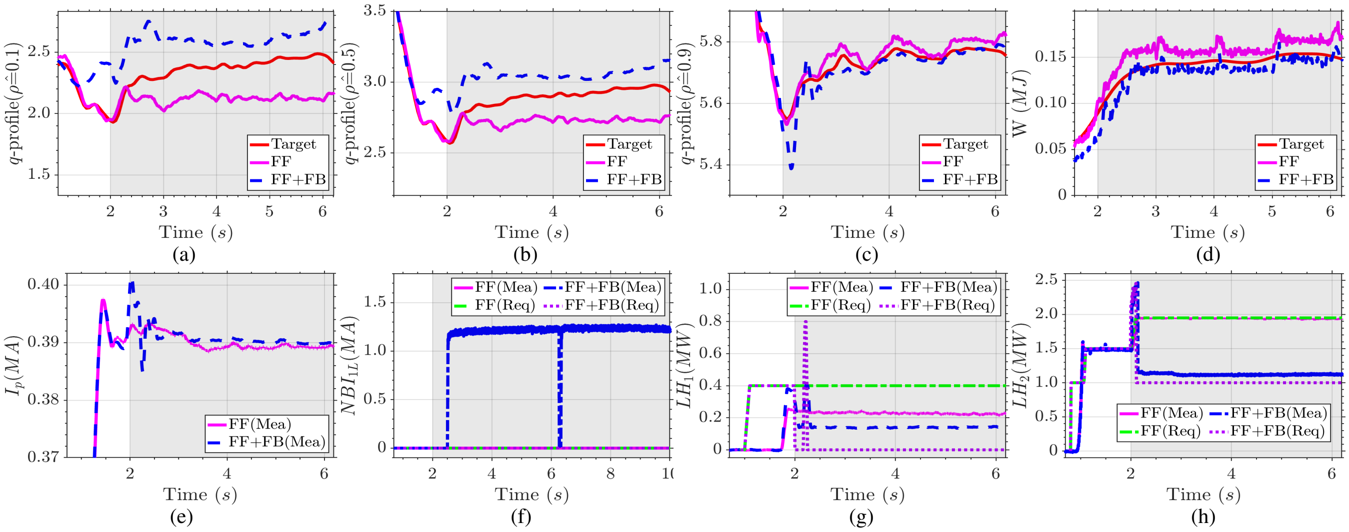

Fig. 2. EAST experimental results (#103739). Time evolutions of the target, feedforward-only (FF), and feedforward + feedback (FF+FB) controlled q-profile at three points in space: (a) $\hat{\rho} = 0.1$, (b) $\hat{\rho} = 0.5$, and (c) $\hat{\rho} = 0.9$. Time evolutions of the target, FF and FF+FB plasma stored energy: (d) W. Time evolutions of actuators ((e) I_p, (f) 2.45 GHz lower hybrid power, (g) 4.60 GHz lower hybrid power, and (h) neutral beams 1L) are plotted for both FF and FF+FB discharges. White region: feedback off; light gray region: feedback on.

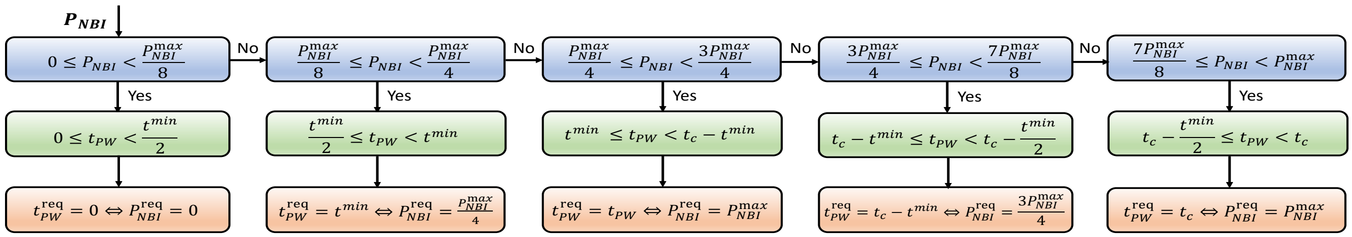

Fig. 3. PWM algorithm. The minimum on-time t_{on}^{min} and minimum off-time t_{off}^{min} are identical, i.e. $t_{on}^{min} = t_{off}^{min} \triangleq t^{min}$. Moreover, $t_c = 4t^{min}$ is assumed.

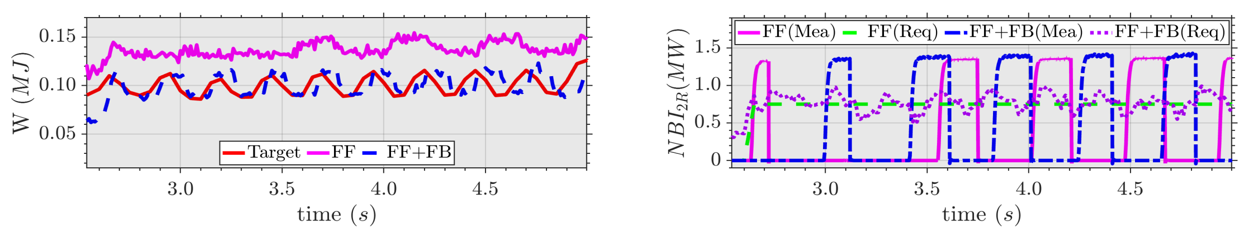

Fig. 4. EAST experimental results (#114118). Time evolutions of the target, feedforward-only (FF), and feedforward + feedback (FF+FB) controlled plasma stored energy: (left) W. Time evolution of actuator: (right) neutral beams 2R is plotted for both FF and FF+FB discharges.

REFERENCES

[1] J. Barton, M. Boyer, W. Shi and E. Schuster, "Toroidal current profile control during low confinement mode plasma discharges in DIII-D via first-principles-driven model-based robust control synthesis," *Nucl. Fusion*, vol. 52, p. 123018, 2012.

[2] H. Wang and E. Schuster, "Robust control of the current profile and plasma energy in EAST," *Fusion Engineering and Design*, vol. 146, pp. 688–691, 2019.

[3] S. Wang, E. Witrant, and D. Moreau, "Robust control of q-profile and βp using data-driven models on EAST," *Fusion Engineering and Design*, vol. 162, p. 112071, 2021.

[4] M. Boyer, J. Barton, E. Schuster and others, "First-principles-driven model-based current profile control for the DIII-D tokamak via LQI optimal control," *Plasma Phys. Control. Fusion*, vol. 55, p. 105007, 2013.

[5] Z. Wang, H. Wang, E. Schuster, Z. Luo, Y. Huang, Q. Yuan, B. Xiao, and D. Humphreys, "Optimal shaping of the safety factor profile in the EAST tokamak," in *2021 IEEE Conference on Control Technology and Applications (CCTA)*. IEEE, 2021, pp. 63–68.

[6] B. Mavkov, E. Witrant, C. Prieur, E. Maljaars, F. Felici, O. Sauter, *et al.*, "Experimental validation of a lyapunov-based controller for the plasma safety factor and plasma pressure in the TCV tokamak," *Nuclear Fusion*, vol. 58, no. 5, p. 056011, 2018.

[7] A. Pajares and E. Schuster, "Current profile and normalized beta control via feedback linearization and Lyapunov techniques," *Nuclear Fusion*, vol. 61, no. 3, p. 036006, 2021.

[8] Y. Ou, E. Schuster, T. C. Luce, J. R. Ferron, M. L. Walker, and D. A. Humphreys, "Receding-horizon optimal control of the current profile evolution during the ramp-up phase of a tokamak discharge," *Control Engineering Practice*, vol. 19, pp. 22–31, 2011.

[9] E. Maljaars, F. Felici, T. Blanken, C. Galperti, O. Sauter, *et al.*, "Profile control simulations and experiments on TCV: a controller test environment and results using a model-based predictive controller," *Nuclear Fusion*, vol. 57, no. 12, p. 126063, 2017.

[10] H. Wang, W. P. Wehner, and E. Schuster, "Combined current profile and plasma energy control via model predictive control in the EAST tokamak," in *2018 26th Mediterranean Conference on Control and Automation (MED)*. IEEE, 2018, pp. 1–9.

[11] J. Barton, W. Shi, *et al.*, "Physics-based control-oriented modeling of the current density profile dynamics in high-performance tokamak plasmas," in *52nd IEEE International Conference on Decision and Control*, 2013.

[12] Y. Huang, B. Xiao, Z. Luo, Q. Yuan, *et al.*, "Implementation of GPU parallel equilibrium reconstruction for plasma control in EAST," *Fusion Engineering and Design*, vol. 112, pp. 1019–1024, 2016.

[13] ITER EDA *et al.*, "ITER Physics Basis Editors," *Nuclear Fusion*, vol. 39, no. 12, pp. 2201–2215, 1999.